This is an open access article published under an ACS AuthorChoice License, which permits copying and redistribution of the article or any adaptations for non-commercial purposes.

THE JOURNAL OF PHYSICAL CHEMISTRY C

Article

pubs.acs.org/JPCC

Spin-State Effects on the Thermal Dihydrogen Release from Solid-State $[MH(\eta^2\text{-}H_2)dppe_2]^+$ (M = Fe, Ru, Os) Organometallic Complexes for Hydrogen Storage Applications

David G. Abrecht, Jorge A. Muñoz, Hillary L. Smith, and Brent Fultz*

W. M. Keck Laboratory, California Institute of Technology, 1200 East California Boulevard, MC 138-78, Pasadena, California 91125, United States

Supporting Information

ABSTRACT: Mössbauer spectroscopy, experimental thermodynamic measurements, and computational studies were performed to investigate the properties of molecular hydrogen binding to the organometallic fragments $[MHdppe_2]^+$ (M = Fe, Ru, Os; dppe =1,2-bis(diphenylphosphino)ethane) to form the dihydrogen complex fragments $[MH(\eta^2\text{-}H_2)dppe_2]^+$. Mössbauer spectroscopy showed that the dehydrogenated complex $[FeHdppe_2]^+$ adopts a geometry consistent with the triplet spin state, transitioning to a singlet state complex upon addition of the dihydrogen molecule in a manner similar to the previously studied dinitrogen complexes. From simulations, this spin transition behavior was found to be responsible for the strong binding behavior experimentally observed in the iron complex. Spin-singlet to spin-singlet transitions were found to exhibit thermodynamics consistent with the 5d > 3d > 4d binding trend observed for other transition metal dihydrogen complexes. Finally, the method for distinguishing between dihydrogen and dihydride complexes based on partial quadrupole splittings observed in Mössbauer spectra was confirmed, providing a tool for further characterization of these unique species for Mössbauer active compounds.

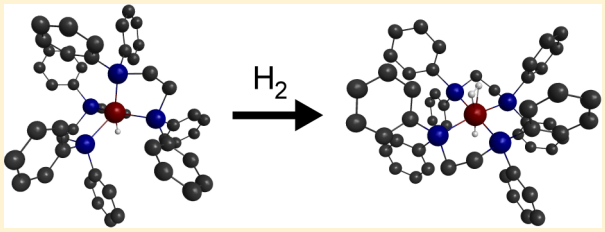

Hydrogen fuel, as a clean-burning, renewable replacement for petroleum-based automotive fuels, has the potential to mitigate vehicle pollution, improve overall vehicle efficiencies,[1] and reduce our dependence on increasingly costly petroleum production. However, before hydrogen-fueled vehicles can become widely commercialized, technologies must be developed to allow storage of sufficient quantities of hydrogen onboard to achieve comparable ranges to modern liquid-fueled vehicles.[2] This need has led to the development of several classes of solid-state storage materials, including metal and complex hydrides, ammonia borane and amides, activated carbons, and metal−organic frameworks, that bind hydrogen in a condensed form, increasing the volumetric energy density of the fuel system at moderate temperatures and pressures to achieve operating conditions amenable to the operation of the vehicle safely and economically.[3−5]

Two mechanisms dominate the interactions of these storage materials with hydrogen gas: chemical absorption, where the hydrogen molecule is dissociated and hydrogen atoms are bound to the solid through strong chemical interactions, and physisorption, where the hydrogen molecule is bound weakly to the solid through dispersion forces. Unfortunately, while interaction strengths vary within each class, typical interaction strength ranges for chemical absorption and physisorption lie outside of the ideal thermodynamic range for storage system behavior, generally described by an absorption entropy of 131 J/mol-K and an absorption enthalpy of 25−60 kJ/mol.[6,7] Ongoing research efforts have focused on the modification of these solid systems[8−10] or the development of new materials to achieve the thermodynamic "middle-ground" between these two interaction mechanisms. Hydrogen ligation (or Kubas binding), a third interaction type in which hydrogen binds chemically to an unsaturated metal center without dissociation to form a dihydrogen−metal three-center bond, is expected to provide such a thermodynamic middle-ground for hydrogen binding that would be useful to producing practical materials. Such interactions were originally associated with hydrogen binding in metal−organic frameworks with unsaturated metal centers.[11,12] While this behavior has since been disproven by examination of the electronic exchange interaction occurring in similar metal−organic frameworks,[13−15] interest in Kubas-type binding has remained for hydrogen storage applications and has led to renewed experimental and theoretical efforts to develop materials exhibiting this effect.[16−18]

Investigations of the thermodynamic properties of hydrogen ligation in typical hydrogen storage materials are often hindered by the presence of additional standard physisorption processes that make up the majority of the hydrogen-solid interactions, and thermodynamic investigations of these binding interactions in the basic chemical literature remain sparse. To facilitate an improved understanding of how these materials may be utilized in materials design applications, we performed thermodynamic

Received: September 30, 2013
Revised: January 2, 2014
Published: January 7, 2014

 © 2014 American Chemical Society dx.doi.org/10.1021/jp409739b | J. Phys. Chem. C 2014, 118, 1783−1792

and mechanistic analyses on the Kubas interactions in materials that exhibit hydrogen ligation as the primary absorption process. In our previous work,[19] we investigated the thermodynamics of Kubas binding in $[Mn(CO)dppe_2][BArF^{24}]$ (where dppe denotes 1,2-bis(diphenylphosphino)ethane) and its group 7 analogues. We found that the Langmuir isotherm model accurately described the experimental behavior for hydrogen absorption in this complex, allowing for a simple determination of the thermodynamic properties through application of the van't Hoff equation, and revealing a large absorption enthalpy of $\Delta H = -52.2$ kJ/mol and a comparatively small absorption entropy of $\Delta S = -99.6$ J/mol·K. Electronic structure simulations of hydrogen absorption over the fragment $[Mn(CO)dppe_2]^+$ were successful in quantitatively reproducing the experimental behavior and thermodynamic properties, and simulations were used to extend the analysis to the other group 7 metal fragments $[Tc(CO)dppe_2]^+$ and $[Re(CO)dppe_2]^+$ to develop trends for the hydrogen absorption behavior within the periodic table.

In this work, we extend the analysis to describe the thermodynamics of hydrogen binding to the isoelectronic organometallic fragments $[MHdppe_2]^+$ (M = Fe, Ru, Os) to form the dihydrogen complexes $[MH(\eta^2\text{-}H_2)dppe_2]^+$. The group 8 complexes containing the cationic fragment $[MH(\eta^2\text{-}H_2)dppe_2]^+$ (M = Fe, Ru, Os) are among the most well-studied dihydrogen compounds available in the literature. The crystal structures for all three dihydrogen complexes have been determined by X-ray diffraction[20−23] and found to be isostructural, and neutron diffraction experiments have been performed for the iron and ruthenium complexes to determine dihydrogen positions.[20,21] Extensive NMR work has been performed[24] to examine the dynamics of dihydrogen exchange, heterolytic cleavage, and intramolecular exchange of the hydride and dihydrogen within all three dihydrogen complexes. Multiple spectroscopic studies have been performed to characterize the iron complex, including Mössbauer spectroscopy[25] and analysis of the vibrational modes through inelastic neutron scattering.[26]

Thermodynamic properties of the dihydrogen interaction with the metal center in these complexes remain undetermined, largely because of the high stability of the dihydrogen products and strong reactivity of the five-coordinate species in the iron and osmium compounds that prevent characterization. While Mössbauer, UV−vis and IR spectroscopy have been reported for the directly synthesized five-coordinate iron complex[27] and H_2/D_2 exchange has been shown to occur through a stable intermediate,[24] the thermal decomposition products of the iron and osmium species have not been directly identified and have only been assigned through the analogous $[RuHdppe_2]^+$ cation, which is stable at room temperature. No characterization studies have been reported for $[OsHdppe_2]^+$ or $[RuHdppe_2]^+$ complexes, despite the stability of the ruthenium species.

Identification of the complexes involved in reversible hydrogen absorption is the first step required for accurate thermodynamic simulations. Mössbauer spectroscopy, in particular, provides a probe of the valence and spin state of the central iron atom in iron complexes, as well as a measure of the charge transfer between the metal center and attached ligands. The availability of this information and the atomic selectivity of the technique makes Mössbauer spectroscopy uniquely suited for investigating group 8 dihydrogen complexes, and for determining mechanisms in Kubas binding. Evidence for the identification of the thermal decomposition product of $[FeH(\eta^2\text{-}H_2)dppe_2][NTf_2]$ (NTf_2 = bis(trifluoromethlysulfonyl)imide) through Mössbauer spectroscopy and other techniques is presented below, and simulated thermodynamic parameters are reported for the hydrogen binding interaction in the group 8 fragments $[MH(\eta^2\text{-}H_2)dppe_2]^+$ (M = Fe, Ru, Os).

EXPERIMENTAL SECTION

Unless otherwise stated, all reactions were performed under a dinitrogen atmosphere using either a controlled-atmosphere glovebox or Schlenck line techniques. 1,2-bis(diphenylphosphino)ethane (dppe) was purchased from Strem Chemicals and used without further purification. Crystalline bis(trifluoro-methanesulfonyl)imide was purchased from Acros Organics and used without further purification. Research-grade gases were purchased from Matheson and used directly. All solvents were dried and deoxygenated by purging with dry dinitrogen gas for 15 min before passing through packed columns of activated alumina and activated copper. After synthesis, materials were stored under dry argon in an atmosphere-controlled glovebox until their use in testing.

Solution-state NMR spectra were recorded on a Varian 300 MHz instrument with ^1H shifts reported relative to the residual solvent peak, and ^{31}P peaks reported relative to 85% H_3PO_4. Deuterated NMR solvents were purchased from Cambridge Isotopes Laboratories. Deuterated benzene was purified by vacuum distillation from a sodium/benzophenone solution before use. Deuterated bromobenzene was dried over CaH_2 and vacuum distilled before use.

Preparation of *cis*-FeH_2dppe_2. This procedure was a modification of existing literature procedures.[24,28] Anhydrous $FeCl_2$ (319.8 mg, 2.523 mmol) was suspended in 2 mL of tetrahydrofuran (THF). A solution of 1,2-bis(diphenylphosphino)ethane (2.0052 g, 5.033 mmol) in 6 mL THF was added, and the suspension was stirred until a milky white precipitate formed. $NaBH_4$ (220.0 mg, 5.680 mmol) in 8 mL of dry ethanol was then added, producing strong outgassing and causing all components to immediately dissolve to form a dark red solution. The solution was stirred for 3 h during which outgassing continued and a yellow powder precipitated. The remaining solution was decanted from the precipitate, and the precipitate was dissolved in benzene and filtered over Celite to remove salt impurities. Removal of the solvent in vacuo produced the product as a fine yellow powder. Yield 1.8533 g (73.5% on iron). ^1H NMR spectra was broad, indicating a fluxional molecule. ^1H NMR (300 MHz) in C_6D_6: δ −12.76 (quad., 2H); 1.80 (s, 4H); 2.14 (s, 2H); 2.40 (s, 2H); 6.44 (s, 4H); 6.58−7.12 (m, 20H); 7.14−7.80 (m, 12H); 8.67 (s, 4H). ^{31}P NMR (300 MHz) in C_6D_6: δ 91.5 (s); 103.3 (s).

Preparation of $[FeH(\eta^2\text{-}H_2)dppe_2][NTf_2]$. This procedure was a modification of an existing literature procedure.[24] Bis(trifluoromethylsulfonyl)imide (327.8 mg, 1.166 mmol) in 5 mL diethyl ether was added to a solution of *cis*-FeH_2dppe_2 (1.015 g, 1.188 mmol) in 12 mL diethyl ether and allowed to stir for 1 h, forming a light green precipitate. The precipitate was filtered over a medium frit and washed twice with diethyl ether. Removal of residual diethyl ether *in vacuo* produced the product as a light green powder. Yield 1.098 mg (81.8% on iron). N_2 coordination products resulting from the reaction conditions were removed by exposure of the product to 1 atm H_2 gas at room temperature after an initial round of thermal treatment as described below. ^1H NMR (300 MHz) in C_6D_5Br: δ −12.61 (s, broad, 1H); −7.76 (s, broad, 2H); 2.13 (s, 8H);

dx.doi.org/10.1021/jp409739b | J. Phys. Chem. C 2014, 118, 1783−1792

7.16−7.51 (m, 40H). ^{31}P NMR (300 MHz) in C_6D_5Br: δ 92.0 (s).

Thermal Decomposition of [FeH(η^2-H_2)dppe$_2$][NTf$_2$]. [FeH(η^2-H_2)dppe$_2$][NTf$_2$] was placed under vacuum and heated at 125° for 12 h. All as-synthesized samples underwent one initial treatment under these conditions to remove N_2 contaminants and the starting material was regenerated by exposure of the product to 1 atm H_2 gas at room temperature. An additional decomposition cycle was then performed for Mössbauer studies. The resulting blue-green powder was extremely reactive to all available solvents, forming a red-purple solution on contact and preventing NMR characterization.

Mössbauer Spectroscopy. Isotopically enriched [^{57}FeH(η^2-H_2)dppe$_2$][NTf$_2$] and its thermal decomposition products were made according to the procedures above. ^{57}Fe metal was purchased from Isoflex USA. $^{57}FeCl_2$ was made by reacting shavings of ^{57}Fe (0.13 mg, 0.228 mmol) metal with excess concentrated hydrochloric acid (1.0 mL, 12M) in 5 mL methanol. The resulting yellow solution was reduced and dried at 160° under vacuum for 8 h to produce the anhydrous starting material. Unenriched $FeCl_2{\cdot}4H_2O$ was purchased from Alfa Aesar for testing of $FeCl_2$ species. Dehydrated $FeCl_2{\cdot}2H_2O$ and anhydrous $FeCl_2$ samples were produced from this material by heating at 300 °C under vacuum for 6 h.

Organometallic samples were loaded into a custom-built, O-ring sealed PTFE sample cell under an argon atmosphere. Sealed samples were stable for up to 24 h in air at room temperature. Spectra were recorded over six hours in the transmission configuration using a gas-filled proportional counter and source radiation from the decay of ^{57}Co in a rhodium matrix. As-received and dehydrated $FeCl_2$ samples were sealed in a Kapton sample cell with Kapton tape under an argon atmosphere and measured for 24 h in the transmission configuration using a Si solid-state detector. Isomer shifts are referenced to bcc iron for all samples.

Kinetic Isotherms. Kinetic isotherms were recorded for the thermal release of the H_2 ligand from [FeH(η^2-H_2)dppe$_2$][NTf$_2$] using a custom-built Sieverts apparatus. Solid [FeH(η^2-H_2)dppe$_2$][NTf$_2$] (257 mg) was loaded into a 14 mL stainless steel reactor under an argon atmosphere and sealed before transfer to the instrument. Swagelok VCR copper filter gaskets with 2 μm stainless steel filters were used to prevent loss of the powdered sample from the reactor during measurements. After transferring the reactor to the assembly, samples were allowed to pump down overnight to 3.1×10^{-7} Torr at the pump inlet before measurements were performed.

The rate of hydrogen release was measured by placing the sample under vacuum conditions for nominally 1 h at the desired temperature, followed by expansion of hydrogen gas from a calibrated volume into the reactor. Residual gas mass spectroscopy was performed during the evacuation of the reactor to identify the decomposition products. Ideal gas mole balance was used to determine the quantity reabsorbed after exposure of the degassed sample to 0.5 atm hydrogen gas. Time and pressure resolution of the instrument were 500 ms and 5 Torr, respectively.

Calculations. Electronic structure calculations were performed for the singlet state of the cationic fragments [MH(η^2-H_2)dppe$_2$]$^+$ and [MHdppe$_2$]$^+$ (M = Fe, Ru, Os), and the hydrogen molecule using the GAMESS-US software package.[29] Geometry optimizations for the organometallic fragments were performed using fully spin-restricted (RHF), restricted open-shell (ROHF) and unrestricted (UHF) density functional theory calculations, with the B3LYP exchange-correlation functional[30,31] and the LANL2DZ basis set.[32−35] An additional p polarization shell for light atoms and d polarization shell for heavier atoms were added to augment the basis set. Starting structures for optimizations were taken from X-ray diffraction (XRD) experiments reported previously for [FeH(η^2-H_2)-dppe$_2$][BF_4][23] and on calculated singlet structures[27] for [FeHdppe$_2$]$^+$. Effective core potentials[33−35] representing the core 10 electrons for iron and phosphorus atoms, the core 28 electrons for ruthenium and the core 60 electrons for osmium were used. Self-consistent field (SCF) convergence was set to 5.0×10^{-6} for all calculations. Geometry optimizations were performed to a tolerance of 10^{-4} au.

Thermal corrections to the energy and normal-mode frequencies were obtained from vibrational analysis of the Hessian matrix for each fragment calculated using the B3LYP/LANL2DZ-ECP level of theory with seminumerical methods, with contributions from positive and negative displacements of 0.01 bohr. Partition functions of the fragments, q_{tot} at 1 atm pressure were also obtained from vibrational analysis. A scaling factor of 0.96 was used in calculating thermodynamic properties and normal-mode frequencies to correct known errors in the LANL2DZ basis set, consistent with common practice.[37] Symmetry of the rotational modes was determined by analysis of the components of the mode eigenvector associated with the two hydrogen atoms, and the mode was considered symmetric if the x, y, and z components of the force constants for each atom were of opposite sign and deviated in value by less than 0.1 millidyne/angstrom.

Ab-initio ground state electronic energies were calculated using the spin-component scaled Møller−Plesset second order perturbation[36] (SCS-MP2) scheme with the LANL2DZ-ECP basis set from the RHF optimized geometries found from density functional theory (DFT) calculations. Restricted open-shell Hartree−Fock (ROHF) and unrestricted Hartree−Fock (UHF) ground-state energy calculations were performed similarly using the non-spin-component scaled Møller−Plesset perturbation with the LANL2DZ-ECP basis set on spin-singlet and spin-triplet [FeHdppe$_2$]$^+$ and spin-singlet [FeH(η^2-H_2)-dppe$_2$]$^+$ for comparison of the spin state effects. SCF convergence was set to 5.0×10^{-6} for these calculations, and the second-order gradient tolerance was set to 0.15 au.

The chemical potential of hydrogen gas was calculated from the partition function for the hydrogen molecule through the relationship

$$\mu_{gas}(T, P) = -kT \ln(q_{tot}(T, P^\circ)) + \ln\left(\frac{P}{P^\circ}\right) \quad (1)$$

where k is Boltzmann's constant, T is the temperature in Kelvin, P is the pressure of the system, and P° is the standard pressure of the system, taken to be 1 atm. Rotational degeneracy for the hydrogen molecule is included in the partition function calculated with the GAMESS software.

The energy for each fragment, E, was obtained as the sum of the ground-state energy, ϵ_0, and the thermal correction obtained from vibrational analysis, $\epsilon_{corr}(T)$, which contains contributions from the electronic, translational, vibrational, and rotational motions of the molecule. The binding energy of the hydrogen molecule to the organometallic site, ΔE, was calculated as

$$\Delta E(T) = E_{M-H_2}(T) - E_{H_2}(T) - E_M(T) \quad (2)$$

dx.doi.org/10.1021/jp409739b | J. Phys. Chem. C 2014, 118, 1783−1792

where the subscripts M−H_2, H_2, and M represent the organometallic adduct fragment, hydrogen gas, and the bare organometallic fragment, respectively.

To simulate the Mössbauer parameters for the iron fragments, fully ab initio geometry optimizations and total energy calculations were performed using the TZVP level of theory[38−41] for [FeH(η^2-H_2)dppe$_2$]$^+$ and [FeHdppe$_2$]$^+$, with *p* and *d* polarization shells as described above. Calculations were also performed on the nitroprusside anion, [Fe(NO)(CN)$_5$]$^{2-}$, to be used as a reference state for isomer shifts. Isomer shift and electric quadrupole splitting values were obtained from the electronic charge density and electric field gradient at the iron nucleus according to the method described by Blaha.[42] Isomer shifts were converted from the nitroprusside scale to the bcc iron scale by subtracting 0.257 mm/s.

RESULTS AND DISCUSSION

Mössbauer Spectroscopy. Identification of the decomposition pathway as well as the structure of the presumed five-coordinate product species [FeHdppe$_2$]$^+$ has previously been precluded by the extreme reactivity of the species with solvents and with trace oxygen and moisture, preventing characterization by X-ray diffraction or NMR.[27] To investigate the decomposition pathway further, we performed Mössbauer spectroscopy of thermally decomposed [^{57}FeH(η^2-H_2)dppe$_2$][NTf$_2$] before and after reabsorption of hydrogen to help identify the cycling products. These spectra appear in Figure 1

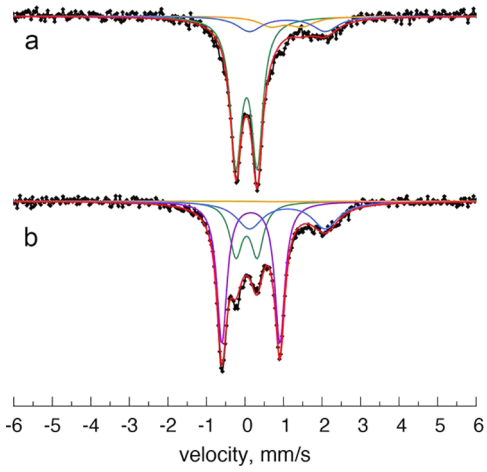

Figure 1. Mössbauer spectra for (a) as synthesized [FeH(η^2-H_2)dppe$_2$][NTf$_2$] after N_2 contaminant removal and rehydrogenation and (b) [FeH(η^2-H_2)dppe$_2$][NTf$_2$] thermally decomposed under vacuum at 125 °C for 12 h. Experimental data (black) overlaid with Lorentzian doublet fits corresponding to [FeH(η^2-H_2)dppe$_2$][NTf$_2$] (green), [FeHdppe$_2$][NTf$_2$] (purple), anhydrous $FeCl_2$ (orange), and $FeCl_2$·$2H_2O$ (blue). The sum of the fits, which minimized the sum of the absolute error with the data, appears in red. $FeCl_2$ and its dihydrate, as residual reactants from the synthesis, account for approximately 25% of the integrated intensity in both spectra.

along with the results of Lorentzian fits to the spectrum. The corresponding values for the isomer shifts and electric quadrupole splittings, along with the literature values for the directly synthesized [FeH(η^2-H_2)dppe$_2$][BF$_4$] and [FeHdppe$_2$][BPh$_4$], appear in Table 1.

Only partial decomposition of the dihydrogen complex was observed upon cycling, with the integrated intensities of the Lorentzian fits giving a conversion of approximately 68%.

Table 1. Isomer Shift and Electric Quadrupole Splitting Values of Iron Complexes Obtained from Mössbauer Spectroscopy, in mm/s[a]

complex	IS, mm/s	EQS, mm/s
Experimental		
[FeH(η^2−H_2)dppe$_2$][NTf$_2$]	+0.043	0.552
[FeHdppe$_2$][NTf$_2$]	+0.155	1.510
$FeCl_2$, *anhydrous*	+1.081	0.799
$FeCl_2$·$2H_2O$	+1.103	1.97
$FeCl_2$·$4H_2O$	+1.197	2.97
Simulation		
[FeH(η^2−H_2)dppe$_2$]$^+$	+0.140	−0.777
[FeHdppe$_2$]$^+$, singlet	+0.112	−0.396
[FeHdppe$_2$]$^+$, triplet	+0.208	+1.338
FeH_2dppe$_2$	+0.108	+0.962
[Fe(NO)CN$_5$]$^{2-}$	–	+1.562
Literature Values[25,27,43−46]		
[FeH(η^2−H_2)dppe$_2$][BF$_4$]	+0.384	−0.560
[FeHdppe$_2$][BPh$_4$]	+0.227	1.518
$FeCl_2$	+1.260	0.800
[Fe(NO)CN$_5$]$^{2-}$	–	+1.726

[a]For EQS values, a sign designation is absent if the sign was not determined. The isomer shift of the nitroprusside anion was used as a reference for the simulations and is thus not reported.

Electric quadrupole splitting (EQS) values for the major peaks in the thermally decomposed and reabsorbed samples correspond well to literature values for the five-coordinate species and the H_2 adduct, respectively. EQS values are indicative of perturbations of the electric field around the metal center due to the attached ligands, and are a good indicator of the chemical environment of the first coordination sphere. The similarity of the EQS values to the literature values thus provides strong evidence for the presence of the [FeH(η^2-H_2)dppe$_2$]$^+$ and [FeHdppe$_2$]$^+$ cations in the starting and decomposed sample. Isomer shift (IS) values for the cycled systems show deviations from the literature values, although they remain within the range typically associated with low-spin Fe^{II} complexes. These deviations likely arise from the different choice of counterion used in this study and the associated change in the charge density within the pair. The large EQS value for the [FeHdppe$_2$]$^+$ complex is characteristic of nonbonding electrons in a high-spin d^6 configuration, which correlates with previous Mössbauer measurements and magnetic susceptibility measurements of the [FeHdppe$_2$]$^+$ cation performed by Franke, et al.[27] revealing paramagnetism in the material. The isomer shift of the complex remains within the low-spin Fe (II) regime, suggesting that the typical reduction in the *s*-electron density around the nucleus from the high-spin state is compensated by donation from the attached ligands.

With the crystal structures for [FeHdppe$_2$]$^+$ complexes unavailable from experiments, computational simulations of the Mössbauer parameters were used to help identify the structure and electronic character of the molecule. Ground-state structures of [FeHdppe$_2$]$^+$ in the spin-singlet and spin-triplet states have previously been performed by Franke, et al.,[27] and were reported to be nearly isoenergetic, with the singlet state slightly more favorable. These states were also reported to have different molecular geometries, with the singlet-state molecule having an octahedral geometry while the triplet-state molecule has quadratic-pyramidal geometry. These differing geometries

dx.doi.org/10.1021/jp409739b | J. Phys. Chem. C 2014, 118, 1783−1792

are expected to alter the EQS values due to the broken symmetry of the ligand arrangement in the triplet-state molecule, and thus simulations of the EQS values can allow for direct identification of the spin-state of $[FeHdppe_2]^+$ complexes observed in Mössbauer experiments.

The results of the Mössbauer simulations are given in Table 1. DFT geometry optimization of the singlet and triplet five-coordinate states performed using ab initio calculations with the TZVP basis set were successful in reproducing the structure symmetries originally reported by Franke, et al.[27] Structure visualizations and ground state energies from these calculations are reported in the Supporting Information.

The electric field gradient tensor at the iron nucleus and the isomer shift relative to bcc iron were calculated from the electronic structure of the optimized geometries. EQS values were derived from the principal component of the tensor without consideration of the asymmetry factor and IS values were derived from the electron density at the nucleus according to the method described by Blaha.[42] These values appear in Table 1. The principal component was found to be oriented primarily along the iron-hydride axis in each of the simulations, with a slight skew in the triplet state five-coordinate complex toward the empty coordination site, which no longer aligns with the iron-hydride axis in the quadratic-pyramidal geometry. The expected differentiation in the EQS values between the singlet-state and triplet-state geometries was observed, and the value for the triplet state was found to be consistent with the experimental and literature Mössbauer values for $[FeHdppe_2]^+$. Simulations of the EQS values for singlet $[FeH(\eta^2\text{-}H_2)dppe_2]^+$ and the nitroprusside anion were also performed and were found to correspond well to their experimental values within the expected range of error for simulations of Mössbauer properties.[42] These results provide strong evidence for predominance of the triplet state-configuration of $[FeHdppe_2]^+$ at room temperature. Isomer shift values for both simulations fell within the range for low-spin Fe (II) organometallic complexes and correlated well with the experimental values, but did not display sufficient deviation to distinguish between the two spin configurations, suggesting that there is not a significant difference in the electron density at the iron nucleus between the two states.

Simulations of EQS values allow for determination of the sign of the principal component of the electric field gradient, and correspondingly the sign of the EQS. These signs are presented with their values in Table 1. With identification of the sign, the method of partial quadrupole splittings presented by Bancroft[47] can be used to determine the individual contribution of the H_2 ligand to the EQS from the experimental value. The expression for the EQS based on partial quadrupole splittings (Q) is

$$\mathrm{EQS} = \sum_i Q(L_i)(3\cos^2\theta_i - 1) \tag{3}$$

where $Q(L_i)$ is the partial quadrupole splitting of ligand i, and θ_i is the angle the ligand−metal bond makes with the principal component axis of the electric field gradient. Assuming perfect octahedral geometry and the principal axis aligned along the H−Fe−H_2 axis, the expression for the EQS becomes

$$\mathrm{EQS} = 2Q(H^-) + 2Q(H_2) - 4Q(\mathrm{dppe}/2) \tag{4}$$

Using the values of $Q(H^-) = -1.04$ mm/s and $Q(\mathrm{dppe}/2) = -0.50$ mm/s, this expression leads to a value of $Q(H_2) = -0.245$ mm/s, which correlates well with the value of −0.22 mm/s presented by Morris and Schlaf for $[FeH(\eta^2\text{-}H_2)dppe_2][BF_4]$.[25] The low Q value of dihydrogen as a ligand, compared to the large value of the hydride ligand, should be universal for Fe (II) organometallic complexes because of the additive nature of the partial quadrupole splitting model. This distinct feature of dihydrogen as a ligand may be useful for identifying dihydrogen complexes and Kubas binding in Mössbauer active materials, as well as defining the onset of dihydrogen-dihydride transitions.

The Mössbauer spectra also indicate that significant quantities of $FeCl_2$ remaining unreacted within the isotopically enriched samples, with both anhydrous and dihydrate species accounting for approximately 25% of the total integrated intensity. This is likely due to incomplete mixing in the small scale vessels used to produce the material, leading to colloidal $FeCl_2$ within the THF mixture during complexation with the dppe ligand. This issue is a known problem of this synthetic route, in the past leading to erroneous identification of the species $[FeCl_2dppe_2]$. Barclay,[43] et al. discussed this in detail, and also identified the individual species through Mössbauer spectroscopy. In our experiments, the residual $FeCl_2$ within the sample appears to have been beneficial, preferentially scavenging trace water to protect the dehydrogenated species during measurements, as the anhydrous material is completely converted during the thermal decomposition cycle. This effect also places a bound on the hygroscopic affinity of the decomposition product, since $FeCl_2$ was preferentially hydrated.

Thermodynamics. Thermodynamic isotherms using the Sieverts technique, such as those measured for the isoelectronic manganese complexes reported previously,[19] were attempted but could not be obtained for $[FeH(\eta^2\text{-}H_2)dppe_2][NTf_2]$ because reversible equilibrium pressures from the complex were below the experimentally detectable level of 5 Torr for all temperatures up to 420 K. At 420 K, the complex decomposed irreversibly, releasing a large quantity of hydrogen gas and producing a black solid containing multiple phosphorus peaks and a complex proton spectrum in NMR measurements, indicating multiple decomposition products.

Reversible release of dihydrogen from the complex was observable below 420 K by residual gas mass spectroscopy (see Supporting Information) and by reabsorption of hydrogen gas onto the sample as determined by mole balance in the Sieverts apparatus. Based on these observations, kinetic rates of desorption of dihydrogen from the hydrogenated complex were measured between 350 and 410 K, and the results are shown in Figure 2. An Arrhenius fit to the kinetic data gives an activation energy of $E_A = 32.3$ kJ/mol for the release process. Assuming a simple decomposition scheme and extrapolating the kinetic data to 298 K gives a value of 2.98×10^{-6} s^{-1} for the decomposition rate constant, which indicates a significant barrier to hydrogen release and a significantly lower release rate than reported for $W(\eta^2\text{-}H_2)(CO)_3(PCy_3)_2$ in solution.[48]

Reabsorption at all temperatures took place from 0.5 atm H_2 overpressure in less than the 500 ms time resolution of the instrument, indicating the absence of diffusional barriers and a strong driving force for reabsorption in the sample, but otherwise preventing direct measurement of the absorption rates. This absence of diffusional barriers in the reabsorption suggests that the slow release rate is intrinsic to the decomposition process, which along with the previously reported results for $W(CO)_3(PCy_3)_2$, indicates a wide range

dx.doi.org/10.1021/jp409739b | J. Phys. Chem. C 2014, 118, 1783−1792

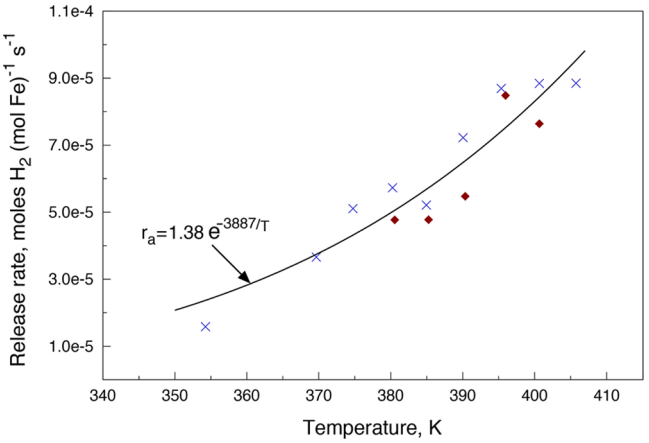

Figure 2. Kinetic measurements for hydrogen release from the reversible thermal decomposition of $[FeH(\eta^2\text{-}H_2)dppe_2][NTf_2]$. The sample was heated to the temperature shown under 0.5 atm hydrogen gas, then exposed to dynamic vacuum for nominally 1 h before re-exposure to a known quantity of hydrogen gas to establish the quantity released. All data points were acquired on the same sample through multiple thermal decomposition cycles. For the nth decomposition cycle, blue crosses (×) correspond to $T_n > T_{n-1}$, and red diamonds (◆) correspond to $T_n < T_{n-1}$. An Arrhenius fit gives E_A = 32.3 kJ/mol, R^2 = 0.8659.

of activation energies are possible for hydrogen release in dihydrogen complexes.

During the course of kinetic testing, the samples underwent multiple absorption/desorption cycles without observed loss of capacity, as shown in Figure 2. This consistency supports a simple decomposition and reabsorption scheme and a lack of formation of stable side products or multiple reaction pathways, in accordance with the Mössbauer results.

To investigate the thermodynamic properties of the absorption reaction, simulations of the Langmuir absorption behavior onto the singlet-state complexes $[MHdppe_2]^+$ (M = Fe, Ru, Os) were performed, based on the previously observed behavior for the isothermal manganese complexes.[19] However, an additional complication to the absorption behavior arises in complexes containing a hydride *trans* to the dihydrogen binding site. Dissociation of the bound dihydrogen molecule and recombination in the resulting trihydride $[MH_3dppe_2]^+$ can lead to inversion of the binding site within the molecule. Bautista et al.[24] found through solution-state NMR experiments that this behavior is present and occurs rapidly in the iron cation $[FeH(\eta^2\text{-}H_2)dppe_2]^+$ and its osmium analogue, but did not observe the behavior significantly in the ruthenium analogue. This inversion would have no effect on the bulk binding properties of H_2 on the molecular level or on the system in solution, where the orientation of the molecules is randomized. However, in the solid-state, where the relative orientation of the molecules is fixed, the configuration of molecules with original and inverted binding site geometries can lead to additional entropic effects that must be taken into consideration in modeling the binding.

To address the entropy arising from the inversion potential of the molecules, an adjustment to the formulation of the partition function used in the statistical Langmuir isotherm[19] can be performed. Because the unbound states are unable to alter their configuration, this inversion only affects the entropy of the bound states. The partition function describing this behavior can be formulated by assigning an orientation to the hydrogen molecules, such that "up" or "down" molecules bind to the open site with equivalent binding energies. The partition function for the system can then be expressed as

$$\Xi = \sum_{n_\uparrow}^{N} \sum_{n_\downarrow}^{N-n_\uparrow} \frac{N!}{n_\uparrow! n_\downarrow! (N - n_\uparrow - n_\downarrow)!} e^{-\beta \Delta E(n_\downarrow + n_\uparrow)} e^{\beta \mu_{gas}(n_\downarrow + n_\uparrow)} \tag{5}$$

where the subscript arrows denote the orientation of the binding molecule, with the total number of bound dihydrogen molecules $n = n_\downarrow + n_\uparrow$. From this partition function, a new Langmuir isotherm can be derived, giving

$$\frac{\langle n \rangle}{N} = \frac{2q_s e^{\beta(\mu_{gas} - \Delta E)}}{1 + 2q_s e^{\beta(\mu_{gas} - \Delta E)}} \tag{6}$$

The modified isotherm, given in eq 6 was used for iron and osmium complex absorption simulations, whereas a standard statistical Langmuir isotherm was used for the ruthenium complex. The numerical prefactor of two before the exponentials in eq 6 is the only difference between the equation for the invertible iron and osmium complexes and the noninvertible ruthenium complex, and represents the increase in the available system configurations from invertibility. Analysis of the rotational mode eigenvector components indicated that the rotation of the H_2 molecule about its center of mass was asymmetric for all of the complexes, and a value of q_s = 1 was used for all simulations.

As with the group 7 complexes, the vibrational analysis revealed that occupied normal modes of the hydrogen molecule in the group 8 H_2 adducts were dominated by the rotational modes, with frequencies of 385.7, 385.5, and 202.1 cm^{-1} for Fe, Ru, and Os species, respectively. The rotational mode at 385.7 cm^{-1} for the iron complex was previously assigned by Eckert et al.[26] as a translation mode based on the presence of additional peaks at 225 and 255 cm^{-1} in the vibration spectra from inelastic neutron scattering experiments. These lower energy peaks were also reproduced by the GAMESS simulations at 237.6 and 254.3 cm^{-1}, and were found to be associated with strong translation modes of the iron center toward the hydride, which couple to both the hydride and the dihydrogen atoms. The broad peak at 400 cm^{-1} in the neutron scattering experiment thus likely corresponds to the primary rotational mode of the dihydrogen molecule.

Although evidence for square-pyramidal geometries of five-coordinate ruthenium(II) hydride complexes with tetraphosphine ligands exists, the strong NMR signals observed in these studies suggests that these molecules are diamagnetic and thus in the singlet state,[49−51] and that the square-pyramidal geometries reported are a result of the electronic and steric effects of the ligands. Unfortunately, geometric investigations of species with the specific ligands in our study are unavailable from NMR studies because of the high affinity of the uncoordinated site for solvent molecules.[27,49] For the purpose of investigating periodic trends, we therefore make the assumption that the ruthenium and osmium complexes being studied show analogous geometries to their iron analogue. Simulations of singlet-state complexes with octahedral geometries were first performed to establish trends down the periodic table in the absence of spin effects. The standard enthalpy and entropy obtained from the K_{eq} values of the simulated Langmuir isotherms are given in Table 2. As with the group 6 complexes reported by Gonzalez and Hoff[52] and the

dx.doi.org/10.1021/jp409739b | J. Phys. Chem. C 2014, 118, 1783−1792

Table 2. Spin-Component Corrected Energies, Enthalpies, and Entropies of the H_2 Absorption Reaction to the Spin-Singlet Species at 1 atm, 298 K, and Rotational Entropy of the Bound States at 298 K and 373 K[a]

compound	$\Delta E°$	$\Delta H°$	$\Delta S°$	S_{rot} (298 K)	S_{rot} (373 K)
$[FeH(\eta^2-H_2)dppe_2]^+$	−41.2	−48.0	−91.4	4.19	5.74
$[RuH(\eta^2-H_2)dppe_2]^+$	−33.9	−41.4	−98.5	4.19	5.74
$[OsH(\eta^2-H_2)dppe_2]^+$	−76.3	−80.6	−82.9	8.76	10.59

[a]Energy and enthalpy values are given in kJ/mol, and entropy values are given in J/mol·K.

group 7 complexes reported by Abrecht and Fultz,[19] the binding enthalpy in the singlet state group 8 complexes increases as 5d > 3d > 4d. Interestingly, the difference between the enthalpies and entropies of the osmium species and the other group 8 complexes is much higher than the corresponding differences in the group 6 and 7 complexes. This result suggests stronger back-donation from the osmium center and stabilization of the trihydride species, which is consistent with the reported NMR studies in solution.[24]

Simulated singlet-state thermodynamic values and isotherms for the osmium and ruthenium complexes correlate well with qualitative observations of the stabilities of the dihydrogen complexes.[24] $[OsH(\eta^2\text{-}H_2)dppe_2]^+$ was found to be extremely stable to loss of the dihydrogen ligand at all temperatures, with greater than 97% coverage down to 0.25 Torr at 373 K. This behavior is also consistent with observations of exchange kinetics in the complex by Bautista et al., which indicate that $[OsH(\eta^2\text{-}H_2)dppe_2][BF_4]$ is highly stable to exchange of the H_2 ligand with N_2, D_2, or CH_3CN in the solid state or in solution. Simulated isotherms for absorption over the ruthenium complex are presented in Figure 3. As shown in the figure,

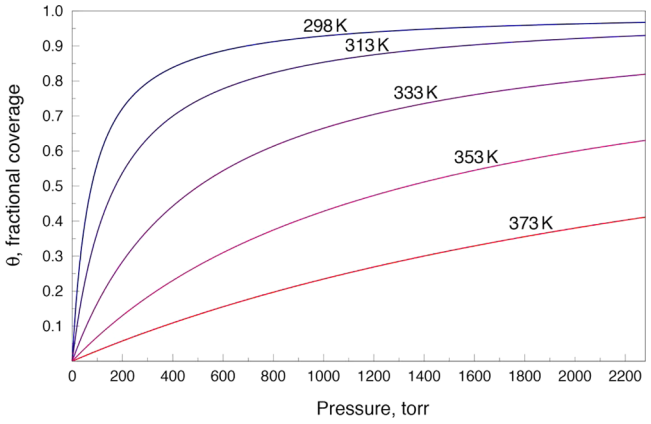

Figure 3. Simulated Langmuir isotherms for hydrogen absorption onto $[RuHdppe_2]^+$ up to 2280 Torr (3 bar) hydrogen pressure.

the ruthenium complex has only ~90% coverage at room temperature and 1.0 atm H_2 pressure, and rapidly loses coordination of the dihydrogen complex at increasing temperatures. This behavior indicates significant overpressure is required to maintain the dihydrogen complex, consistent with experimental reports of the instability of the complex over time at room temperature.

The absorption enthalpy for the singlet iron fragment $[FeHdppe_2]^+$ is lower than that of the manganese[19] fragment $[Mn(CO)dppe_2]^+$, which significantly underestimates the binding strength in the iron complex relative to our experimental observations and reported behavior in the solid state, suggesting a strong effect on the binding enthalpy due to spin effects despite previous reports of the nearly isoenergetic nature of the singlet and triplet states for the iron complex.[27] To investigate this effect further, MP2 calculations were performed on $[FeHdppe_2]^+$ in both the singlet and triplet states using the LANL2DZ-ECP basis set using the ROHF and UHF shell approximations. The results are given in Table 3

Table 3. Spin-Component Uncorrected MP2 Level Energies, Enthalpies, and Entropies of the H_2 Absorption Reaction onto $[FeHdppe_2]^+$ at 1 atm, 298 K, to Form Spin-Singlet $[FeH(\eta^2\text{-}H_2)dppe_2]^+$[a]

		$\Delta E°$	$\Delta H°$	$\Delta S°$
RHF				
	singlet - H_2	−72.98	−66.08	−91.36
ROHF				
	singlet - H_2	−129.48	−122.58	−91.38
	triplet - H_2	−51.15	−44.94	−91.41
	singlet → triplet		−77.64	0.03
UHF				
	singlet - H_2	−73.12	−65.88	−91.32
	triplet - H_2	−828.97	−822.07	−99.45
	singlet → triplet		756.19	8.13

[a]Singlet/triplet designation indicates the state of the five-coordinate species. Energy and enthalpy values were calculated from the same vibrational analysis, and are given in kJ/mol, and entropy values are given in J/mol·K.

along with the uncorrected MP2 values from the initial RHF calculations. As shown, UHF calculations greatly overestimate the magnitude of the binding enthalpy, suggesting complete irreversibility of the H_2 absorption until decomposition of the complex. The UHF calculations also resulted in a singlet ground state for the five-coordinate complex, which contradicts the results of the Mössbauer experiments. We thus discounted the UHF results as likely suffering from errors due to significant spin contamination within such a large molecule. ROHF calculations, despite not reproducing the original RHF ground-state energy for the singlet state, provide both the correct triplet ground-state of the five-coordinate species and a negative hydrogen absorption enthalpy and free energy. These values, however, do not predict the increased binding strength for the direct binding of hydrogen to triplet-state five-coordinate species. We thus conclude that the hydrogen release must occur between the hydrogenated complex to the singlet-state, which then rapidly converts to the more favorable triplet-state configuration, accounting for the differences in observed behavior between the iron and ruthenium complexes. This transition must also occur more rapidly than the Mössbauer time scale for the iron complex, since the singlet species was not observed. However, because of the issues associated with calculating reaction thermodynamics from DFT for non-isopiestic reactions, these values should not be taken as quantitative.

Such spin state transitions may be responsible for other complications known to exist selectively in iron dihydrogen complexes. For instance, Bianchini et al.[53,54] found that during

dx.doi.org/10.1021/jp409739b | J. Phys. Chem. C 2014, 118, 1783−1792

the catalysis of alkyne hydrogenation, the tetraphoshine complex $[(PP_3)FeH(H_2)][BPh_4]$ (PP_3 = $P(CH_2CH_2PPh_2)$) preferentially removes a phosphine arm before releasing the dihydrogen ligand, while the ruthenium analogue $[(PP_3)RuH(H_2)][BPh_4]$ first releases the dihydrogen molecule for the same catalytic process. If present in the tetraphosphine complexes, the loss of hydrogen to form a high-energy singlet state may be less favorable than the removal of a phosphine arm, and this effect would not be present in the analogous ruthenium complex. Recently Coronado, et al.[55] also detailed the spin-crossover effects in the iron-based metal−organic framework $[Fe(btzx)_3]ClO_4$ (btzx =1,4-bis(tetrazol-1-ylmethyl)benzene) upon CO_2 adsorption, which showed a unique magnetic transition for CO_2 that was not present for N_2 adsorption. Such unique spin-dependent reactions may be useful for engineered materials for gas absorption reactions.

CONCLUSIONS

Mössbauer spectroscopy has been used to probe the thermal release of H_2 from $[FeH(\eta^2\text{-}H_2)dppe_2]$ $[NTf_2]$, and experimental results were compared to electronic structure simulations using the GAMESS-US software. Release of the dihydrogen molecule from the complex to form the triplet-state complex $[FeHdppe_2][NTf_2]$ through the intermediate singlet-state complex was found to be the predominant dehydrogenation mechanism at 125 °C, with the accompanying singlet→triplet magnetic transition greatly affecting the thermodynamic stability of the hydrogen adduct. A partial quadrupole splitting value of −0.245 mm/s was confirmed for the dihydrogen ligand in these complexes, which differs significantly from the value of −1.04 mm/s for hydride ligands, and may be used to help distinguish bound dihydrogen molecules from dihydrides.

A modification of the statistical Langmuir isotherm model was applied to the absorption of hydrogen onto the singlet-state organometallic fragments $[MHdppe_2]^+$ (M = Fe, Ru, Os) and the triplet-state fragment $[FeHdppe_2]^+$. This model accurately described the reported behavior for the ruthenium and osmium complexes. The model also described the magnitude of the spin-state transition on the absorption behavior in the iron complex, which showed singlet-state enthalpy values similar to the manganese complex reported previously, despite experimental evidence for much stronger binding. Singlet-state absorption enthalpies demonstrated the familiar increasing periodic trend of 5d > 3d > 4d, indicating a consistency within the isoelectronic transition metal species exhibiting the same spin state. However, the magnitude of the differences between the metal centers was significantly different in the group 8 complexes, particularly for the osmium complex. Simulation of hydrogen binding to the triplet-state using restricted open-shell Hartree−Fock calculations qualitatively confirmed the triplet ground state and indicated that the increase in binding enthalpy was likely due to the necessity of forming the spin-singlet intermediate, providing an explanation for the anomalous experimental results. Such strong spin-state effects on the hydrogen binding properties in Kubas complexes may be useful in developing unique materials for hydrogen reactions.

ASSOCIATED CONTENT

Supporting Information

Residual gas mass spectroscopy results from H_2 desorption experiments, structural representations, and full values for the energy calculations are available as Supporting Information. This material is available free of charge via the Internet at http://pubs.acs.org.

AUTHOR INFORMATION

Corresponding Author

*E-mail: btf@caltech.edu.

Notes

The authors declare no competing financial interest.

ACKNOWLEDGMENTS

The authors wish to thank David Vandervelde of Caltech's liquid NMR facility for his assistance with NMR experiments and Joseph Reiter and Jason Zan at the Jet Propulsion Laboratory in Pasadena, CA for their assistance in planning thermodynamic measurements. Sieverts instrument work was performed at the Jet Propulsion Laboratory, which is operated by the California Institute of Technology under contract with NASA. The Caltech NMR facility is partially supported by the National Institutes of Health through Grant NIH RR027690. ROHF calculations were performed using computational facilities located at the National Energy Research Scientific Computing (NERSC) Center, which is supported by the Office of Science of the U.S. Department of Energy under Contract No. DE-AC02-05CH11231. We wish to express gratitude to the Resnick Sustainability Institute for financial support of the project. This work was supported as part of EFree, an Energy Frontier Research Center, under Award No. DE-SG0001057.

REFERENCES

(1) Zamel, N.; Li, X. Life Cycle Analysis of Vehicles Powered by a Fuel Cell and by Internal Combustion Engine for Canada. *J. Power Sources* **2006**, *155*, 297−310.

(2) Yang, J.; Sudik, A.; Wolverton, C.; Siegel, D. J. High Capacity Hydrogen Storage Materials: Attributes for Automotive Applications and Techniques for Materials Discovery. *Chem. Soc. Rev.* **2010**, *39*, 656−675.

(3) Klebanoff, L.; Keller, J. *Final Report for the DOE Metal Hydrides Center of Excellence*; SAND2012-0786; Sandia National Laboratories: Albuquerque, NM, 2012.

(4) Ott, K. *Final Report for the DOE Chemical Hydrogen Storage Center of Excellence*; LA-UR-20074; Los Alamos National Laboratory: Los Alamos, NM, 2012.

(5) Simpson, L. *Hydrogen Sorption Center of Excellence Final Report*; National Renewable Energy Laboratory: Golden, CO, 2012.

(6) Satyapal, S.; Petrovic, J.; Read, C.; Thomas, G.; Ordaz, G. The U.S. Department of Energy's National Hydrogen Storage Project: Progress towards Meeting Hydrogen-Powered Vehicle Requirements. *Catal. Today* **2007**, *120*, 246−256.

(7) Akbarzadeh, A. R.; Wolverton, C.; Ozolins, V. First-Principles Determination of Crystal Structures, Phase Stability, and Reaction Thermodynamics in the Li−Mg−Al−H Hydrogen Storage System. *Phys. Rev. B* **2009**, *79*, 184102.

(8) Ozolins, V.; Majzoub, E. H.; Wolverton, C. First-Principles Prediction of Thermodynamically Reversible Hydrogen Storage Reactions in the Li−Mg−Ca−B−H System. *J. Am. Chem. Soc.* **2009**, *131*, 230−237.

(9) Vajo, J. J.; Mertens, F.; Ahn, C. C.; Bowman, R. C., Jr.; Fultz, B. Altering Hydrogen Storage Properties by Hydride Destabilization through Alloy Formation: LiH and MgH_2 Destabilized Si. *J. Phys. Chem. B* **2004**, *108*, 13977−13983.

(10) Liu, Y.; Brown, C. M.; Neumann, D. A.; Geohegan, D. B.; Puretzky, A. A.; Rouleau, C. M.; Hu, H.; Styers-Barnett, D.; Krasnov, P. O.; Yakobson, B. I. Metal-Assisted Hydrogen Storage on Pt-Decorated Single-Walled Carbon Nanohorns. *Carbon* **2012**, *50*, 4953−4964.

(11) Dinca, M.; Long, J. R. Hydrogen Storage in Microporous Metal−Organic Frameworks with Exposed Metal Sites. *Angew. Chem., Int. Ed.* **2008**, *47*, 6766−6779.
(12) Hoang, T. K. A.; Antonelli, D. M. Exploiting the Kubas Interaction in the Design of Hydrogen Storage Materials. *Adv. Mater.* **2009**, *21*, 1787−1800.
(13) Brown, C. M.; Liu, Y.; Yildirim, T.; Peterson, V. K.; Kepert, C. J. Hydrogen Adsorption in HKUST-1: A Combined Inelastic Neutron Scattering and First-Principles Study. *Nanotechnology* **2009**, *20*, 204025.
(14) Kong, L.; Román-Pérez, G.; Soler, J. M.; Langreth, D. C. Energetics and Dynamics of H_2 Adsorbed in a Nanoporous Material at Low Temperature. *Phys. Rev. Lett.* **2009**, *103*, 096103.
(15) Zhou, W.; Yildirim, T. Nature and Tunability of Enhanced Hydrogen Binding in Metal−Organic Frameworks with Exposed Transition Metal Sites. *J. Phys. Chem. C* **2008**, *112*, 8132−8135.
(16) Skipper, C. V. J.; Hamaed, A.; Antonelli, D. M.; Kaltsoyannis, N. Computational Study of Silica-Supported Transition Metal Fragments for Kubas-Type Hydrogen Storage. *J. Am. Chem. Soc.* **2010**, *132*, 17296−17305.
(17) Hamaed, A.; Hoang, T. K. A.; Moula, G.; Aroca, R.; Trudeau, M. L.; Antonelli, D. M. Hydride-Induced Amplification of Performance and Binding Enthalpies in Chromium Hydrazide Gels for Kubas-Type Hydrogen Storage. *J. Am. Chem. Soc.* **2011**, *113*, 15434−15443.
(18) Hoang, T. K. A.; Antonelli, D. M. Exploiting the Kubas Interaction in the Design of Hydrogen Storage Materials. *Adv. Mater.* **2009**, *21*, 1787−1800.
(19) Abrecht, D. G.; Fultz, B. Evaluation of the Thermodynamic Properties of H_2 Binding in Solid State Dihydrogen Complexes $[M(\eta^2\text{-}H_2)(CO)dppe_2][BArF^{24}]$ (M = Mn, Tc, Re): An Experimental and First Principles Study. *J. Phys. Chem. C* **2012**, *116*, 22245−22252.
(20) Ricci, J. S.; Koetzle, T. F.; Bautista, M. T.; Hofstede, T. M.; Morris, R. H.; Sawyer, J. F. Single-Crystal X-ray and Neutron Diffraction Studies of an η^2-Dihydrogen Transition-Metal Complex: *trans*-$[Fe(\eta^2\text{-}H_2)(H)(PPh_2CH_2CH_2PPh_2)_2]BPh_4$. *J. Am. Chem. Soc.* **1989**, *111*, 8823−8827.
(21) Albinati, A.; Klooster, W. T.; Koetzle, T. F.; Fortin, J. B.; Ricci, J. S.; Eckert, J.; Fong, T. P.; Lough, A. J.; Morris, R. H.; Golombek, A. P. Single-Crystal X-ray and Neutron Diffraction Structure Determination and Inelastic Neutron Scattering Study of the Dihydrogen Complex *trans*-$[Ru(H_2)(H)(dppe)_2][BPh_4]$. *Inorg. Chim. Acta* **1997**, *259*, 351−357.
(22) Farrar, D. H.; Maltby, P. A.; Morris, R. H. Structure of *trans*-$[OsH(\eta^2\text{-}H_2)(PPh_2CH_2CH_2PPh_2)_2][BF_4]$. *Acta Crystallogr.* **1992**, *C48*, 28−31.
(23) Morris, R. H.; Sawyer, J. F.; Shiralian, M.; Zubkowski, J. D. Two Molecular Hydrogen Complexes: *trans*-$[M(\eta^2\text{-}H_2)(H)(PPh_2CH_2CH_2PPh_2)_2]BF_4$ (M = Fe, Ru). The Crystal Structure Determination of the Iron Complex. *J. Am. Chem. Soc.* **1985**, *107*, 5581−5582.
(24) Bautista, M. T.; Capellani, E. P.; Drouin, S. D.; Morris, R. H.; Schweitzer, C. T.; Sella, A.; Zubkowski, J. Preparation and Spectroscopic Properties of the η^2-Dihydrogen Complexes $[MH(\eta^2\text{-}H_2)(PR_2CH_2CH_2PR_2)_2]^+$ (M = Fe, Ru; R = Ph, Et) and Trends in Properties down the Iron Group Triad. *J. Am. Chem. Soc.* **1991**, *113*, 4876−4887.
(25) Morris, R. H.; Schlaf, M. π-Bonding of the Dihydrogen Ligand Probed by Mössbauer Spectroscopy. *Inorg. Chem.* **1994**, *33*, 1725−1726.
(26) Eckert, J.; Blank, H.; Bautista, M. T.; Morris, R. H. Dynamics of Molecular Hydrogen in the Complex *trans*-$[Fe(\eta^2\text{-}H_2)(H)(PPh_2CH_2CH_2PPh_2)_2]BF_4$ in the Solid State as Revealed by Neutron-Scattering Experiments. *Inorg. Chem.* **1990**, *29*, 747−750.
(27) Franke, O.; Wiesler, B. E.; Lehnert, N.; Peters, G.; Burger, P.; Tuczek, F. The Iron Hydrido Complex $[FeH(dppe)_2]^+$: Solution and Solid-State Reactivity with Dinitrogen. *Z. Anorg. Allg. Chem.* **2006**, *632*, 1247−1256.
(28) Hills, A.; Hughes, D. L.; Jimenez-Tenorio, M.; Leigh, G. J. Complexes of Tertiary Phosphines with Iron(II) and Dinitrogen, Dihydrogen, and Other Small Molecules. *J. Organomet. Chem.* **1990**, *391*, C41−C44.
(29) Schmidt, M. W.; Baldridge, K. K.; Boatz, J. A.; Elbert, S. T.; Gordon, M. S.; Jensen, J. H.; Koseki, S.; Matsunaga, N.; Nguyen, K. A.; Su, S.; et al. General Atomic and Molecular Electronic Structure System. *J. Comput. Chem.* **1993**, *14*, 1347−1363.
(30) Becke, A. D. Density-Functional Thermochemistry. III. The Role of Exact Exchange. *J. Chem. Phys.* **1993**, *98*, 5648.
(31) Lee, C.; Yang, W.; Parr, R. G. Development of the Colle−Salvetti Correlation-Energy Formula into a Functional of the Electron Density. *Phys. Rev. B.* **1988**, *37*, 785−789.
(32) Dunning, Jr., T. H.; Hay, P. J. *Methods of Electronic Structure Theory*; Schaefer , H. F., III, Ed.; Plenum Press: New York, 1977; Vol. 2.
(33) Hay, P. J.; Wadt, W. R. *Ab-Initio* Effective Core Potentials for Molecular Calculations. Potentials for the Transition Metal Atoms Sc to Hg. *J. Chem. Phys.* **1985**, *82*, 270.
(34) Hay, P. J.; Wadt, W. R. *Ab-Initio* Effective Core Potentials for Molecular Calculations. Potentials for K to Au Including the Outermost Core Orbitals. *J. Chem. Phys.* **1985**, *82*, 299.
(35) Hay, P. J.; Wadt, W. R. *Ab-Initio* Effective Core Potentials for Molecular Calculations. Potentials for Main Group Elements Na to Bi. *J. Chem. Phys.* **1985**, *82*, 284.
(36) Grimme, S. Improved Second-Order Mø ller-Plesset Perturbation Theory by Separate Scaling of Parallel- and Antiparallel-Spin Pair Correlation Energies. *J. Chem. Phys.* **2003**, *118*, 9095.
(37) NIST Computational Chemistry Comparison and Benchmark Database. NIST Standard Reference Database Number 101, Release 15b , August 2011. Editor: Russell, D., III. http://cccbdb.nist.gov/ (accessed Nov. 24, 2013).
(38) Dunning, T. H., Jr. Gaussian Basis Sets for Use in Correlated Molecular Calculations. III. Contraction of (10s6p) Atomic Basis Sets for the First-Row Atoms. *J. Chem. Phys.* **1971**, *55*, 716.
(39) McLean, A. D.; Chandler, G. S. Contracted Gaussian Basis Sets for Molecular Calculations. I. Second-Row Atoms, Z = 11−18. *J. Chem. Phys.* **1980**, *72*, 5639.
(40) Wachters, A. J. H. Gaussian Basis Set for Molecular Wavefunctions Containing Third-Row Atoms. *J. Chem. Phys.* **1970**, *52*, 1033.
(41) Rappe, A. K.; Smedley, T.; Goddard, W. A., III. Flexible d Basis Sets for Scandium through Copper. *J. Phys. Chem.* **1981**, *85*, 2607−2611.
(42) Blaha, P. Calculations of Mössbauer Parameters in Solids by DFT Bandstructure Calculations. *J. Phys.: Conf. Ser.* **2010**, *217*, 012009.
(43) Barclay, J. E.; Leigh, J. G.; Houlton, A.; Silver, J. Mössbauer and Preparative Studies of Some Iron (II) Complexes of Diphosphines. *J. Chem. Soc., Dalton Trans.* **1988**, *11*, 2865−2870.
(44) Parish, R. V.; Riley, B. F. Studies in Mössbauer Spectrscopy. Part 12. Characterization of Complexes Containing Iron-Silicon Bonds. *J. Chem. Soc., Dalton Trans.* **1979**, 482−487.
(45) Ono, K.; Ito, A.; Fujita, T. The Mössbauer Study of the Ferrous Ion in $FeCl_2$. *J. Phys. Soc. Jpn.* **1964**, *19*, 2119−2126.
(46) Spijkerman, J. J.; Snediker, D. K.; Ruegg, F. C.; DeVoe, J. R. *Standard Reference Materials: Mossbauer Spectroscopy Standard for the Chemical Shift of Iron Compounds*; NBS Misc. Publ. 260−13; United States National Bureau of Standards: Washington, D.C., 1967.
(47) Bancroft, G. M.; Libbey, E. T. Bonding Properties of Ligands: A Mössbauer Study of Carbonyl Complexes of Iron(II). *J. Chem. Soc., Dalton Trans.* **1973**, 2103−2111.
(48) Grills, D. C.; van Eldik, R.; Muckerman, J. T.; Fujita, E. Direct Measurements of Rate Constants and Activation Volumes for the Binding of H_2, D_2, N_2, C_2H_4, and CH_3CN to $W(CO)_3(PCy_3)_2$: Theoretical and Experimental Studies with Time-Resolved Step-Scan FTIR and UV-Vis Spectroscopy. *J. Am. Chem. Soc.* **2006**, *128*, 15728−15741.
(49) Ashworth, T. V.; Chalmers, A. A.; Singleton, E. Solution Structure of Five-Coordinate Complexes of Ruthenium (II): Evidence

for a Square-Pyramidal Geometry for the Cations $[RuXL_4]^+$ (X = H, C_2Ph; L = PMe_2Ph). *Inorg. Chem.* **1985**, *24*, 2125−2126.
(50) Ashworth, T. V.; Singleton, E. Ionic Ruthenium (IV) Trihydrides as Intermediates in the Heterolytic Fission of Dihydrogen by Five-Coordinate Hydridoruthenium (II) Cations. Direct Evidence for an Oxidative Addition-Reductive Elimination Pathway. *J. Chem. Soc., Chem. Commun.* **1976**, *18*, 705−706.
(51) Tsukahara, T.; Kawano, H.; Ishii, Y.; Takahashi, T.; Saburi, M.; Uchida, Y.; Akutagawa, S. Preparation and Reactions of a Novel Five-Coordinate Ruthenium Complex $[RuH(BINAP)_2]PF_6$ and Formation of the First Chiral Molecular Hydrogen Complex $[RuH(h^2\text{-}H_2)\text{-}(BINAP_2]PF_6$. *Chem. Lett.* **1988**, 2055−2058.
(52) Gonzalez, A. A.; Hoff, C. D. Entropy of Binding Molecular Hydrogen and Nitrogen in the Complexes $(P(C_6H_11)_3)_2M(CO)_3$ (M = Cr, Mo, W). *Inorg. Chem.* **1989**, *28*, 4295−4297.
(53) Bianchini, C.; Meli, A.; Peruzzini, M.; Frediani, P.; Bohanna, C.; Esteruelas, M. A.; Oro, L. A. Selective Hydrogenation of 1-Alkynes to Alkenes Catalyzed by an Iron (II) *cis*-Hydride h^2-Dihydrogen Complex. A Case of Intermolecular Reaction between η^2-H_2 and s-Vinyl Ligands. *Organometallics* **1992**, *11*, 138−145.
(54) Bianchini, C.; Meli, A.; Peruzzini, M.; Vizza, F.; Zanobini, F.; Frediani, P. A Homogeneous Iron (II) System Capable of Selectivity Catalyzing the Reduction of Terminal Alkynes to Alkenes and Buta-1,3-dienes. *Organometallics* **1989**, *8*, 2080−2082.
(55) Coronado, E.; Giménez-Marqués, M.; Espallargas, M.; Rey, F.; Vitórica-Yrezábal, I. J. Spin-Crossover Modification through Selective CO_2 Sorption. *J. Am. Chem. Soc.* **2013**, *135*, 15986−15989.